WATER RESOURCES RESEARCH, VOL. 35, NO. 1, PAGES 1–16, JANUARY 1999

Asymptotic solutions for solute transport: A formalism for tracer tomography

D. W. Vasco
Berkeley Laboratory, University of California, Berkeley

Akhil Datta-Gupta
Department of Petroleum Engineering, Texas A&M University, College Station

Abstract. An asymptotic approach to the solution of the transport equation, in the limit of rapid spatial and temporal variation, produces an extremely efficient formalism for the inversion of tracer data. The technique provides tracer concentration sensitivities to porosity, permeability, and pressure gradient variations in just a single simulation run. The calculated sensitivities compare well with those derived using a numerical perturbation method, at a fraction of the computational requirements. An application to a conservative tracer test at Hill Air Force Base in Utah indicates the efficiency and utility of the approach for characterizing three-dimensional variations in flow properties. On the basis of tracer concentration histories at 12 multilevel samplers and three extraction wells, some 44 tracer curves in all, significant small-scale variability in permeability is inferred. In general, the permeability is found to decrease as the lower boundary of the aquifer is approached. The permeability trends we find are consistent with tracer swept volume calculations based upon a moment analysis.

1. Introduction

The understanding and analysis of solute transport is becoming increasingly important for a broad spectrum of applications. Predictions of solute transport are important for understanding the evolution of contaminant plumes [*Graham and Mclaughlin*, 1989a, b; *Rubin*, 1991]. Furthermore, tracer migration and tracer tests may be used to infer subsurface variations in hydrologic properties [*Hyndman et al.*, 1994; *Datta-Gupta et al.*, 1995a; *Medina and Carrera*, 1996]. In addition, the chemical interaction of tracers with material in the subsurface can be used as a tool for estimating variations in saturations. For example, partitioning tracers are providing a means to assess the performance of remediation strategies for non–aqueous phase liquids [*Pope et al.*, 1994; *Jin et al.*, 1995; *James et al.*, 1997]. Unfortunately, our ability to fully utilize transport data is still limited by experimental difficulties, incomplete understanding of mechanisms involved in solute transport, and the computational burden.

The computational task is particularly daunting when inverse modeling or the inversion of transport data is involved. The formulation of the inverse problem usually requires the computation of concentration sensitivities to changes in model parameters. That is, we must compute the change in concentration at an observation point induced by a deviation in subsurface hydrologic properties, such as porosity and permeability. There are several approaches for calculating sensitivities and most of these fall into one of three categories: perturbation techniques, direct algorithms, and adjoint state methods [*Yeh*, 1986; *Mclaughlin and Townley*, 1996].

Conceptually, a perturbation approach is the simplest and usually requires the fewest changes in an existing code for concentration calculations. Sensitivities are estimated by simply perturbing a particular parameter by some small amount and noting the change in concentration with respect to the unperturbed case. This methodology requires a number of simulation runs equal to the number of model parameters. The perturbation approach has been used to approximate sensitivities for both inversion of tracer data and for simulation and optimization of groundwater contamination cleanup strategies [*Gorelick et al.*, 1984; *Ahlfeld et al.*, 1986].

In the direct or sensitivity equation method the equations governing the concentration evolution are differentiated to obtain the equations for the sensitivity coefficients. These equations are then solved numerically for the sensitivities. Because there is one equation for each parameter, this approach can require the same order of work as the perturbation technique. However, as *Kabala and Milly* [1990] show, calculations performed during the simulation may be used to significantly reduce the computation but with a corresponding increase in the required computer code modifications. *Knopman and Voss* [1987] used the direct method to study the behavior of sensitivities associated with the one-dimensional advection-dispersion equation. *Ahlfeld et al.* [1988], *Chang et al.* [1992], and *Medina and Carrera* [1996] used this approach to design groundwater remediation strategies.

The adjoint state approach does not solve the sensitivity equations directly but uses them to derive a set of adjoint equations [*Jacquard and Jain*, 1965]. The advantage is that the number of adjoint equations can be significantly smaller than the number of sensitivity equations [*Vemuri and Karplus*, 1969; *Carter et al.*, 1982]. Application of the adjoint approach to the transport problem is difficult because of the coupling of the transport and flow equations and applications are relatively recent [*Samper and Neuman*, 1986; *Ahlfeld et al.*, 1988; *Sun and Yeh*, 1990; *Skaggs and Barry*, 1996].

In this paper we describe an asymptotic formulation which

Paper number 98WR02742.
0043-1397/99/98WR-02742$09.00

has several advantages over existing approaches. First, the technique utilizes an extremely efficient semianalytic approach to transport modeling that is quite fast even for three-dimensional problems [*Datta-Gupta and King*, 1995]. Second, the sensitivities are formulated in terms of one-dimensional integrals of analytic functions along the streamlines. The computation of sensitivities for all model parameters requires only a single simulation run to construct the streamlines and velocity field. An added benefit of this approach is a relationship between the solute arrival time and medium properties which may be used to derive an initial estimate of the model parameters. The approach is similar to techniques widely used in geophysical and medical imaging. Therefore approaches and algorithms from these fields may be helpful in the inversion of transport data.

2. Methodology

In this section we introduce the asymptotic approach for modeling transport. That is, we shall investigate the high-frequency behavior of the solute distribution as a function of time and space. As such, we envision that the concentration propagates as a rather sharp front. Alternative asymptotic approaches have been used to describe solute transport in the limit of long times, giving, for example, traveling wave solutions [*van der Zee*, 1990; *van Duijn and Knabner*, 1992; *Grundy et al.*, 1994; *Jaekel et al.*, 1996]. The high-frequency asymptotic approach presented here produces analytic expression for the sensitivity of solute concentration to variations in porosity, permeability, and pressure gradient along the flow path. The particular asymptotic approach we are about to describe arose as a mathematical connection between geometrical optics and electromagnetic theory [*Kline and Kay*, 1965]. This methodology has proven useful in the analysis of front propagation in general [*Sethian*, 1996], and many of the concepts such as rays and propagating interfaces or discontinuities have direct counterparts in hydrology [*Bear*, 1972]. It is quite likely that many ideas from geometrical optics had their genesis in early work on fluid flow and hydrodynamics [*Robertson*, 1965], thus completing the circle.

2.1. The Evolution Equation for Concentration

Consider the equation governing the evolution of tracer concentration, $C(\mathbf{x}, t)$, as a function of space $\mathbf{x}$ and time t

$$\frac{\partial C(\mathbf{x}, t)}{\partial t} = \nabla \cdot [\mathbf{D}(\mathbf{x}) \cdot \nabla C(\mathbf{x}, t)] - \frac{\mathbf{q}}{n(\mathbf{x})} \cdot \nabla C(\mathbf{x}, t) \tag{1}$$

where $\mathbf{D}(\mathbf{x})$ denotes the dispersion tensor, $n(\mathbf{x})$ represents the porosity distribution, and $\mathbf{q}$ is the velocity [*Gelhar and Collins*, 1971; *Bear*, 1972]. Now the velocity is related to the permeability $K(\mathbf{x})$ and pressure gradient $\nabla\phi(\mathbf{x})$,

$$\mathbf{q} = -K(\mathbf{x})\nabla\phi(\mathbf{x})$$

so the equation may be rewritten

$$\frac{\partial C(\mathbf{x}, t)}{\partial t} = \nabla \cdot [\mathbf{D}(\mathbf{x}) \cdot \nabla C(\mathbf{x}, t)] + \frac{K(\mathbf{x})\nabla\phi(\mathbf{x})}{n(\mathbf{x})} \cdot \nabla C(\mathbf{x}, t).$$

Let

$$-\frac{K(\mathbf{x})\nabla\phi(\mathbf{x})}{n(\mathbf{x})} = a(\mathbf{x})\mathbf{u} \tag{2}$$

where $\mathbf{u}$ denotes a unit vector in the direction of $\nabla\phi(\mathbf{x})$ and $a(\mathbf{x})$ denotes the magnitude of the vector: $K(\mathbf{x})|\nabla\phi(\mathbf{x})|/n(\mathbf{x})$. For clarity of exposition, we shall consider the dispersion $\mathbf{D}(\mathbf{x})$ to be characterized by a single scalar magnitude, and the partial differential equation then may be written

$$\frac{\partial C(\mathbf{x}, t)}{\partial t} = D\nabla^2 C(\mathbf{x}, t) - a(\mathbf{x})\mathbf{u} \cdot \nabla C(\mathbf{x}, t). \tag{3}$$

2.2. Asymptotic Solutions for Transport

Our solution of (3) will be in the form of a sum of inverse powers of frequency ω, an asymptotic expansion [*Fatemi et al.*, 1995]:

$$C(\mathbf{x}, t) = e^{i\omega\sigma(\mathbf{x},t)} \sum_{n=0}^{\infty} c_n(\mathbf{x}, t)(i\omega)^{-n} \tag{4}$$

Asymptotic expansions or representations have been used extensively in the study of electromagnetic [*Kline and Kay*, 1965] and seismic [*Cerveny et al.*, 1978] wave propagation. The advantage of this form of expansion is that the initial terms of the series represent rapidly varying (high-frequency, large ω) components of the solution and successive terms are associated with lower-frequency behavior. Hence the propagation of a sharp concentration front is described by the initial terms of the sum. For example, the concentration front amplitude is given by

$$|C(\mathbf{x}, t)|^2 = c_0^2(\mathbf{x}, t) + [c_1^2(\mathbf{x}, t) + 2c_0(\mathbf{x}, t)c_2(\mathbf{x}, t)]\omega^{-2} + O(\omega^{-4}). \tag{5}$$

Hence the term $c_0(\mathbf{x}, t)$ is a good approximation to the amplitude for a sharp (high-frequency, large ω) propagating front. In the following section we shall see that the term $\sigma(\mathbf{x}, t)$, known as the phase, governs the geometry of the concentration front.

Substituting the series expansion of (4) into (3) governing the evolution of $C(\mathbf{x}, t)$ produces a relationship between infinite sums. However, we may consider terms of particular orders in ω. The result is an infinite number of equations for the phase $\sigma(\mathbf{x}, t)$ and the series of terms $c_n(\mathbf{x}, t)$, $n = 0, 1, \cdots, \infty$. For example, consider terms of order ω^2,

$$D[\sigma_{x_1}^2(\mathbf{x}, t) + \sigma_{x_2}^2(\mathbf{x}, t) + \sigma_{x_3}^2(\mathbf{x}, t)] = 0 \tag{6}$$

where $\sigma_{x_i}(\mathbf{x}, t)$ denotes $\partial\sigma(\mathbf{x}, t)/\partial x_i$ and the components of the vector $\mathbf{x} = (x_1, x_2, x_3)$ correspond to x, y, and z. Equation (6) implies that for nonzero D, the front's phase contains imaginary as well as real components. From (4) we see that this results in exponentially decreasing concentration with propagation. Physically, this means that the concentration cannot propagate as a sharp front in the presence of dispersion D. Rather, the concentration amplitude decays along the streamlines. We can still carry the analysis forward but we must instead work with isoconcentration surfaces. Because we are interested in illustrating the asymptotic approach and associated concepts, with the fewest additional complications, we shall assume that the dispersion D is negligible. For field-scale solute transport, as presented in our application below, this is a justifiable assumption since the macroscopic mixing is primarily due to convective velocity variations arising from subsurface heterogeneity [*Gelhar and Axness*, 1983; *Lake*, 1989].

2.3. The Eikonal Equation, Trajectories, and Travel Times

Next, consider the equation associated with terms of first order in ω, under the assumption that $D = 0$,

$$c_0(\mathbf{x}, t)\sigma_t(\mathbf{x}, t) = -c_0(\mathbf{x}, t)[a(\mathbf{x})\mathbf{u} \cdot \nabla\sigma(\mathbf{x}, t)]$$

where $\sigma_t(\mathbf{x}, t)$ denotes the partial derivative of $\sigma(\mathbf{x}, t)$ with respect to time. Since we are interested in $\sigma(\mathbf{x}, t)$ on the concentration front, where $c_0(\mathbf{x}, t)$ does not vanish, we have

$$\sigma_t(\mathbf{x}, t) = -a(\mathbf{x})\mathbf{u} \cdot \nabla\sigma(\mathbf{x}, t). \tag{7}$$

Taking absolute values, noting that $|\mathbf{u}\cdot\nabla\sigma| = |\mathbf{u}||\nabla\sigma| \cos\theta$ where θ is the angle between the flow direction and $\nabla\sigma(\mathbf{x}, t)$,

$$|\sigma_t(\mathbf{x}, t)| = |a(\mathbf{x}) \cos\theta||\nabla\sigma(\mathbf{x}, t)|$$

because $\mathbf{u}$ is a unit vector. We may group terms to simplify the above equation

$$s(\mathbf{x})|\sigma_t(\mathbf{x}, t)| = |\nabla\sigma(\mathbf{x}, t)| \tag{8}$$

where $s(\mathbf{x}) = |a(\mathbf{x}) \cos\theta|^{-1}$. Because the concentration front does not intersect itself, we may use the implicit function theorem [*Protter and Morrey*, 1964] to write the phase function (which describes the geometrical evolution of the front) in a separated form. That is, the time and space variations may be separated and $\sigma(\mathbf{x}, t)$ becomes $\sigma(\mathbf{x}, t) = \psi(\mathbf{x}) - t$ [*Kline and Kay*, 1965]. Then $\sigma_t(\mathbf{x}, t) = -1$ and (8) becomes, after squaring,

$$|\nabla\psi(\mathbf{x})|^2 = s^2(\mathbf{x}). \tag{9}$$

Thus the shape of the concentration front is determined by $s(\mathbf{x})$. For a concentration gradient which is perpendicular to the front,

$$s(\mathbf{x}) = n(\mathbf{x})/(K(\mathbf{x})|\nabla\phi(\mathbf{x})|). \tag{10}$$

Equation (9) is a form of the eikonal equation governing the propagation of the concentration front. The eikonal equation appears in many contexts, such as elastic and electromagnetic wave propagation [*Nolet*, 1987; *Kline and Kay*, 1965], and there are now efficient numerical techniques for its solution [*Sethian*, 1996]. One advantage of our description of the concentration front given by (9) is that we can use existing methods, for example, those from medical imaging, to formulate an efficient approach for the inversion of transport data.

The family of concentration fronts define the trajectories, their perpendiculars, and we may use the eikonal equation to calculate concentration trajectories. Consider the family of fronts defined by $\psi(\mathbf{x}) = t$, as given above. Assume that $\psi(\mathbf{x})$ is spatially continuous and has first partial derivatives. This ensures a two-parameter family of orthogonal trajectories to the fronts [*Kline and Kay*, 1965]. Each curve of the family of trajectories will then have direction $\nabla\psi(\mathbf{x})$ at its intersection with $\psi(\mathbf{x}) = t$. Let $x_i = x_i(r)$, $i = 1, 2, 3$ be the equations for the orthogonal trajectories, where r is the distance along the trajectory. Then, since any trajectory is orthogonal to the front, the tangent to the path must be proportional to $\nabla\psi(\mathbf{x})$:

$$\frac{dx_i}{dr} = \lambda(r)\frac{\partial\psi}{\partial x_i}(\mathbf{x}) \qquad i = 1, 2, 3$$

where $\lambda(r)$ is a scaling factor that may be chosen arbitrarily.

From the eikonal equation and the fact that $d\psi(\mathbf{x}) = dt$ it may be shown that the total travel time from the injection source to a point along the trajectory Σ is given by

$$\tau = \int_\Sigma dt = \int_\Sigma s(\mathbf{x})\, dr \tag{11}$$

where Σ denotes that the path of integration is over the trajectory [*Kline and Kay*, 1965]. This expression for travel time is similar to the expression of optical length in geometrical optics [*Kline and Kay*, 1965] as well as seismic travel time [*Nolet*, 1987].

2.4. The Transport Equation and Amplitudes

If terms of order ω^0 are collected in the asymptotic expansion, we produce the transport equation, describing the evolution of $c_0(\mathbf{x}, t)$:

$$\frac{\partial c_0(\mathbf{x}, t)}{\partial t} - D\nabla^2 c_0(\mathbf{x}, t) + a(\mathbf{x})\mathbf{u} \cdot \nabla c_0(\mathbf{x}, t) = 0$$

which is just the original evolution equation (3). In what follows we shall consider convective transport only under the influence of permeability and porosity heterogeneity ($D = 0$). Solutions when dispersion is important may be derived directly from existing one-dimensional solutions [*Gelhar and Collins*, 1971]. For $D = 0$ the equation governing the concentration amplitude becomes

$$\frac{\partial c_0(\mathbf{x}, t)}{\partial t} + a(\mathbf{x})\mathbf{u} \cdot \nabla c_0(\mathbf{x}, t) = 0. \tag{12}$$

This equation simplifies considerably when expressed in terms of travel time coordinates (τ, t) where τ is the travel time to point $\mathbf{x}$ along the streamline, given by equation (11). In terms of these variables

$$\nabla c_0(\tau, t) = \nabla\tau \frac{\partial c_0(\tau, t)}{\partial\tau}$$

and equation (12) becomes

$$\frac{\partial c_0(\tau, t)}{\partial t} + a(\tau)\mathbf{u} \cdot \nabla\tau \frac{\partial c_0(\tau, t)}{\partial\tau} = 0. \tag{13}$$

On noting that $\mathbf{u} \cdot \nabla\tau = s(\tau) = 1/a(\tau)$, (13) simplifies to

$$\frac{\partial c_0(\tau, t)}{\partial t} + \frac{\partial c_0(\tau, t)}{\partial\tau} = 0.$$

For an impulse concentration source in space and time the solution to this equation, given in the original $(\mathbf{x}, t)$ coordinates, is

$$c_0(\mathbf{x}, t) = \delta\left(t - \int_\Sigma s(\mathbf{x})\, dr\right), \tag{14}$$

where $\delta(t)$ denotes the Dirac delta function. For an input concentration at $\mathbf{x} = \mathbf{0}$ with temporal variation $C_0(t)$, the observed concentration is a convolution of the input function with the impulse response of (14); hence

$$c_0(\mathbf{x}, t) = C_0(t - \int_\Sigma s(\mathbf{x})\, dr). \tag{15}$$

2.5. Sensitivities and Transport Tomography

In order to estimate variations in subsurface properties such as porosity $n(\mathbf{x})$ and permeability $K(\mathbf{x})$ from observed variations in transport we must know the change in concentration

induced by changes in these properties. This is accomplished using a perturbation approach in which we consider a small change in $s(\mathbf{x})$, given by equation (10), and calculate the corresponding change in $c_0(\mathbf{x}, t)$. That is, consider an initial spatial distribution of reservoir properties, denoted by $s^0(\mathbf{x})$, and the associated tracer concentration history in this unperturbed medium $c_0^0(\mathbf{x}, t)$. Given a slight perturbation of the initial structure

$$s(\mathbf{x}) = s^0(\mathbf{x}) + \delta s(\mathbf{x}), \tag{16}$$

what is the resulting perturbation in tracer concentration history, $\delta c_0(\mathbf{x}, t)$? Perturbation approaches have been adopted in the inversion of seismic [*Nolet*, 1987] and electromagnetic [*Vasco et al.*, 1997b] arrival times, as well as in the inversion of seismic amplitude data [*Neele et al.*, 1993]. For the moment we shall only consider a perturbation of $s(\mathbf{x})$ which is a composite quantity; shortly we shall decompose this into perturbations of the flow properties: $\delta n(\mathbf{x})$, $\delta K(\mathbf{x})$, and $\delta|\nabla\phi(\mathbf{x})|$. We shall write the tracer concentrations in the perturbed reservoir structure, $c_0(\mathbf{x}, t)$, as a sum,

$$c_0(\mathbf{x}, t) = c_0^0(\mathbf{x}, t) + \delta c_0(\mathbf{x}, t). \tag{17}$$

Consider the form of $c_0(\mathbf{x}, t)$ given in (15):

$$\delta c_0(\mathbf{x}, t) = c_0(\mathbf{x}, t) - c_0^0(\mathbf{x}, t)$$

$$= C_0\left(t - \int_\Sigma [s^0(\mathbf{x}) + \delta s(\mathbf{x})]\, dr\right) - C_0\left(t - \int_{\Sigma_0} s^0(\mathbf{x})\, dr\right). \tag{18}$$

For a small perturbation in medium properties, in the functions comprising $s(\mathbf{x})$, one may show that the perturbation in the trajectory, the change in the original streamline from Σ_0 to the new streamline Σ, is second order in $\delta s(\mathbf{x})$ [*Nolet*, 1987; *King and Datta-Gupta*, 1998]. This fact is related to the often quoted Fermat's principle from optics [*Kline and Kay*, 1965], but it also follows from a linearization of the eikonal equation [*Aldridge*, 1994]. Therefore, to first order, the leading term on the right-hand side may be written

$$C_0\left(t - \int_\Sigma [s^0(\mathbf{x}) + \delta s(\mathbf{x})]\, dr\right)$$

$$= C_0\left(t - \int_{\Sigma_0} s^0(\mathbf{x})\, dr - \int_{\Sigma_0} \delta s(\mathbf{x})\, dr\right).$$

Using a Taylor series expansion and neglecting higher-order terms, this becomes

$$C_0\left(t - \int_\Sigma [s^0(\mathbf{x}) + \delta s(\mathbf{x})]\, dr\right) = C_0\left(t - \int_{\Sigma_0} s^0(\mathbf{x})\, dr\right)$$

$$- C_0'\left(t - \int_{\Sigma_0} s^0(\mathbf{x})\, dr\right)\int_{\Sigma_0} \delta s(\mathbf{x})\, dr$$

where the prime denotes time differentiation. Hence the perturbations in $c_0(\mathbf{x}, t)$ and $s(\mathbf{x})$ are related by

$$\delta c_0(\mathbf{x}, t) = -C_0'\left(t - \int_{\Sigma_0} s^0(\mathbf{x})\, dr\right)\int_{\Sigma_0} \delta s(\mathbf{x})\, dr. \tag{19}$$

Now $s(\mathbf{x})$ is a composite function of the permeability, the porosity, and the pressure gradient:

$$s(\mathbf{x}) = \frac{n(\mathbf{x})}{K(\mathbf{x})|\nabla\phi(\mathbf{x})|} \tag{20}$$

and its variation is given by

$$\delta s(\mathbf{x}) = \frac{\partial s(\mathbf{x})}{\partial K}\,\delta K(\mathbf{x}) + \frac{\partial s(\mathbf{x})}{\partial n}\,\delta n(\mathbf{x}) + \frac{\partial s(\mathbf{x})}{\partial|\nabla\phi|}\,\delta|\nabla\phi(\mathbf{x})|$$

where the partial derivatives are

$$\frac{\partial s(\mathbf{x})}{\partial K} = \frac{-n(\mathbf{x})}{K^2(\mathbf{x})|\nabla\phi(\mathbf{x})|}$$

$$\frac{\partial s(\mathbf{x})}{\partial n} = \frac{1}{K(\mathbf{x})|\nabla\phi(\mathbf{x})|} \tag{21}$$

$$\frac{\partial s(\mathbf{x})}{\partial|\nabla\phi|} = \frac{-n(\mathbf{x})}{K(\mathbf{x})|\nabla\phi(\mathbf{x})|^2}$$

and these quantities are evaluated at the initial model. From (19) the perturbation in concentration due to perturbations in porosity, permeability, and pressure gradient are integrations of the above functions along the trajectory to $\mathbf{x}$. At a producing well a number of trajectories merge and the concentration change is the integral or discretized sum of converging trajectories weighted by $C_0'(t - \int_{\Sigma_0} s^0(\mathbf{x})\, dr)$.

In the preceding derivation we have assumed that dispersion may be neglected. The analysis may be applied when longitudinal dispersion, along streamlines, is included. That is, the perturbation approach is directly applicable to one-dimensional solutions of the advective-dispersion equation as given by *Gelhar and Collins* [1971] and *Bear* [1972]. For example, we may consider a perturbation of the solution of *Gelhar and Collins* [1971]. Written in travel time coordinates for a streamline Σ this solution takes the form

$$C(\mathbf{x}, t) = \frac{1}{\sqrt{4\alpha T(\mathbf{x})}} \exp\left[-(t - \tau(\mathbf{x}))^2/(4\alpha T(\mathbf{x}))\right]$$

where α is the dispersivity and $T(\mathbf{x})$ is the integral

$$T(\mathbf{x}) = \int_\Sigma \frac{dr}{\nu(\mathbf{x})^2}$$

where $\nu(\mathbf{x})$ is the tracer particle velocity. In this manner the tracer inverse problem can be formulated in the presence of longitudinal dispersion.

3. Numerical Calculations

In this section we present numerical calculations based upon the preceding theoretical considerations. First, the asymptotic sensitivities are compared to sensitivities obtained using a perturbation approach. Next, we formulate the linearized inverse problem in terms of a basis function expansion of subsurface properties. That is, a representation of the three-dimensional variations in porosity, permeability, and pressure gradient magnitude in terms of a set of basis functions, such as nonoverlapping cells. An iterative linearized inversion algorithm is then used to infer a two-dimensional permeability distribution based upon a set of synthetic tracer data.

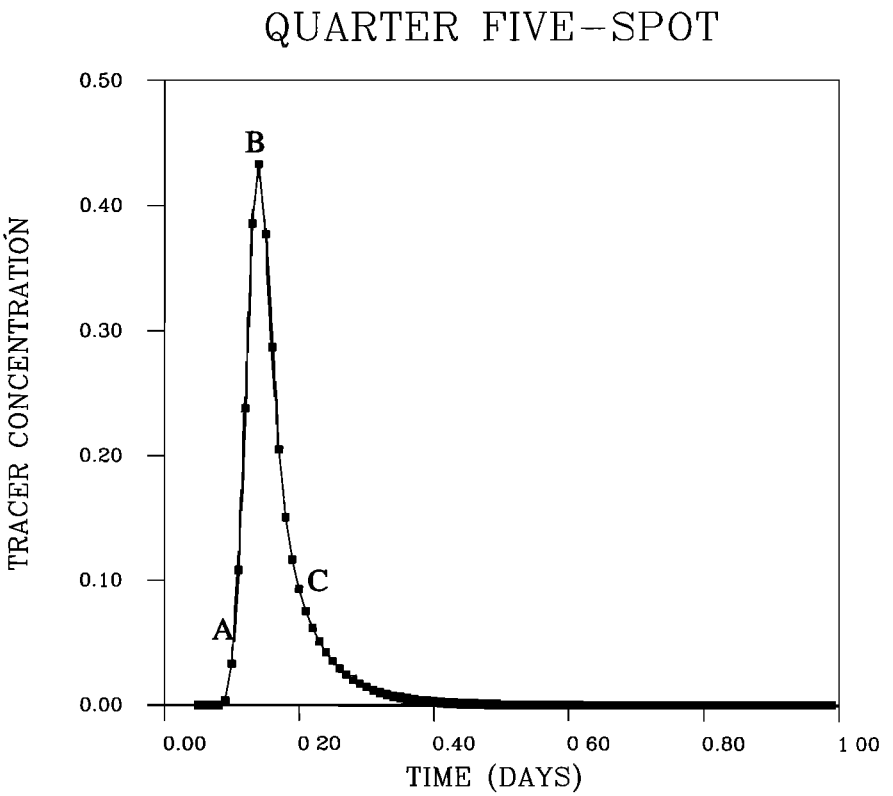

Figure 1. Synthetic tracer data for quarter five-spot sensitivity calculations. The points A, B, and C denote samples for which the sensitivities have been calculated.

3.1. Quarter Five-Spot Sensitivities

As a test of the accuracy of the asymptotic approach, we estimated the sensitivity of tracer concentration to variations in permeability and porosity in a single symmetry element of a five-spot well pattern. An injection well is situated in one corner of a square, while the extraction is from a well in the opposite corner. For simplicity the problem is two-dimensional and all variations are confined to a single plane, the background porosity and permeability distributions are uniform, and all boundaries are closed. The tracer is introduced as a single pulse and the recovered tracer concentration is shown in Figure 1. We shall examine the change in concentration with respect to changes in the spatial distribution of permeability and porosity at three different times, labeled A (0.1 days), B (0.14 days), and C (0.20 days) in this figure.

The sensitivity of tracer concentration to changes in permeability is shown in Plate 1. For these calculations the 100 m by 100 m flow field was subdivided into a 21 by 21 grid of cells, the actual dimensions of the finite difference grid used to calculate the steady state pressure field. The semianalytical streamline simulator of *Datta-Gupta and King* [1995] was used to predict the concentration histories. The numerical estimate of sensitivity was based upon 441 simulations in which each grid block permeability was perturbed by 0.5%. The resulting concentration at each time point was then compared to the calculated concentrations for the unperturbed grid and the concentration deviations are used to compute sensitivities. The sensitivities are displayed such that the concentration change per permeability variation is plotted at the location where the change occurs. Note the implicit pressure dependence in the perturbation approach: The pressure field is changed when the permeability is perturbed. In contrast, the asymptotic expression for permeability sensitivity in (21) does not implicitly include the influence of pressure changes; that effect is contained explicitly in $\partial s(\mathbf{x})/\partial|\nabla\phi|$. The asymptotic sensitivities are computed by integrating the expressions in (19) and (21) over 1000 streamlines. The sensitivities for the perturbation approach (numerical) and the asymptotic approach (streamline) are quite similar overall. The implicit pressure effect is evident in the numerical sensitivities, particularly in the corners of the simulation grid. Computation of the analytic streamline permeability and porosity sensitivities shown in Plates 1 and 2 took just under 6 CPU minutes on a workstation. The corresponding calculation using the conventional perturbation method took a little over 71 CPU minutes per parameter set (porosity, permeability), for a total of 143 CPU minutes.

The general features of the sensitivity distributions agree with earlier computations [*Datta-Gupta et al.*, 1995b; *Vasco et al.*, 1997a]. In particular, for concentrations observed before the peak arrival an increase in permeability between the injection and observation wells results in an increase in concentration. As the concentration front arrives and passes an increase in permeability in the central region between the wells results in a decrease in observed tracer concentration. This behavior corresponds to a shift of the tracer concentration curve forward in time with higher permeability between the wells, resulting in larger concentrations for times just before the peak and lower concentrations for times following the maximum. The mathematical expression of this is the time derivative of the concentration curve in (19).

We also calculated the sensitivity of tracer concentration to variations in porosity using both the perturbation and asymp-

totic approaches. The sensitivities are displayed over the grid of simulation cells in Plate 2. Clearly, the response of concentrations to changes in porosity is opposite in sign to permeability sensitivities. There is a fundamental trade-off between permeability and porosity which is due to the fact that the velocity, $s(\mathbf{x})$, is a function of the ratio of porosity to permeability, as in (20). This highlights the difficulty of simultaneously estimating porosity and permeability variations from concentration data alone. A similar conclusion holds for these parameter distributions and the distribution of pressure gradient magnitudes. Because of the differing functional dependencies on porosity and permeability in (21), the trade-off between porosity and permeability estimates will be less in a heterogeneous background model. Finally, note the larger absolute value of the sensitivity coefficients for porosity relative to those for permeability. This is due to the size of the background values for permeability and porosity; the relative variations in sensitivity coefficients (when scaled by background values) are of the same order.

3.2. Representation of Permeability, Porosity, and Pressure Gradient Variations

In order to use (19), (20), and (21) to infer $K(\mathbf{x})$, $n(\mathbf{x})$, and $|\nabla\phi(\mathbf{x})|$ we require a numerical representation of their spatial variations. For this work our representation will be cell-based and we shall determine the permeability, porosity, and pressure gradients for a collection of grid blocks. More generally, consider an expansion of permeability in terms of an orthogonal set of basis functions, $\beta(\mathbf{x})$, such as rectangular cells, splines, or sinusoidal functions. We can represent the permeability perturbations as a sum of M such basis functions

$$\delta K(\mathbf{x}) = \sum_{m=1}^{M} b_m^K \beta_m(\mathbf{x})$$

where b_m^K are the M expansion coefficients for K, similarly for the other parameters. For rectangular blocks the functions $\beta_m(\mathbf{x})$ may be thought of as functions which vanish outside the cell and have constant values of 1 inside the cell. Substituting the expansions into (21) and (21) into (19), we can consider the contribution of perturbations in the cell properties to variations in concentration. For trajectory i

$$\delta c_0^i(\mathbf{x}, t) = -C_0'\left(t - \int_{\Sigma_i} s^0(\mathbf{x})\, dr\right) \cdot \left(\int_{\Sigma_i} \frac{\partial s(\mathbf{x})}{\partial K} \sum_{m=1}^{M} b_m^K \beta_m(\mathbf{x})\, dr + \int_{\Sigma_i} \frac{\partial s(\mathbf{x})}{\partial n} \sum_{m=1}^{M} b_m^n \beta_m(\mathbf{x})\, dr + \int_{\Sigma_i} \frac{\partial s(\mathbf{x})}{\partial |\nabla\phi|} \sum_{m=1}^{M} b_m^{\nabla\phi} \beta_m(\mathbf{x})\, dr\right). \quad (22)$$

Interchanging summation and integration

$$\delta c_0^i(\mathbf{x}, t) = -\sum_{m=1}^{M} (b_m^K I_{im}^K + b_m^n I_{im}^n + b_m^{\nabla\phi} I_{im}^{|\nabla\phi|}) \quad (23)$$

where

$$I_{im}^K = C_0'\left(t - \int_{\Sigma_i} s^0(\mathbf{x})\, dr\right) \int_{\Sigma_i} \frac{\partial s(\mathbf{x})}{\partial K} \beta_m(\mathbf{x})\, dr$$

$$I_{im}^n = C_0'\left(t - \int_{\Sigma_i} s^0(\mathbf{x})\, dr\right) \int_{\Sigma_i} \frac{\partial s(\mathbf{x})}{\partial n} \beta_m(\mathbf{x})\, dr$$

$$I_{im}^{|\nabla\phi|} = C_0'\left(t - \int_{\Sigma_i} s^0(\mathbf{x})\, dr\right) \int_{\Sigma_i} \frac{\partial s(\mathbf{x})}{\partial |\nabla\phi|} \beta_m(\mathbf{x})\, dr$$

The total response is the weighted summation over all trajectories

$$\delta c_0(\mathbf{x}, t) = \sum_i \delta c_0^i(\mathbf{x}, t)$$

$$= -\sum_i \sum_{m=1}^{M} (b_m^K I_{im}^K + b_m^n I_{im}^n + b_m^{\nabla\phi} I_{im}^{|\nabla\phi|}) \quad (24)$$

Given a collection of concentration histories from various well pairs, we obtain a linear system of equations constraining the permeability and porosity variations and the deviations in pressure gradient

$$\delta\mathbf{c} = \mathbf{M}\mathbf{b} \quad (25)$$

where $\delta\mathbf{c}$ is a vector containing the concentration histories for each well; $\mathbf{M}$ is a matrix with coefficients I_{im}^K, I_{im}^n, and $I_{im}^{|\nabla\phi|}$; and $\mathbf{b}$ is the vector of unknown coefficients $\mathbf{b} = (b_1^K, \cdots, b_M^K, b_1^n, \cdots, b_M^{\nabla\phi})^T$, representing the perturbations in the permeability, porosity, and pressure gradient in each cell. There are numerical algorithms for efficiently solving such linear systems [*Paige and Saunders*, 1982; *Golub and Van Loan*, 1989].

3.3. Inversion of Nine-Spot Synthetic Tracer Data

Some of the issues associated with using tracer data to infer variations in subsurface properties are best illustrated by considering the analysis of a synthetic data set. The inversion of a synthetic data set provides a measure of the optimal performance of our inversion algorithm for a particular configuration of wells and a specific data set. In our test case we considered a nine-spot pattern of boreholes consisting of a central injection well and eight surrounding extraction wells. The distribution of heterogeneity shown in Plate 3a. There is a large, high-permeability region in the southeastern quadrant and an approximately linear low-permeability feature extending from the southwest to the northeast. The central well injected a pulse of tracer, which was observed at the eight extraction wells at the vertices and edges of the nine spot (Plate 3a).

Initially, we attempted to infer permeability variations directly from the concentration histories using an iterative linearized inversion algorithm. That is, the system of linear equations (25) was solved repeatedly for permeability, porosity, and pressure gradient variations which minimize the concentration data residuals. A problem arose when fitting the concentrations directly: If there were secondary peaks in the tracer concentration curve that lay close to the calculated tracer concentration maximum, then the algorithm fit these peaks rather than the matching the synthetic data maximum. Thus matching the concentration curves directly produced local minima, which trapped the inversion. An approach which works in other applications of waveform inversion is to "line up" the curves based upon matching the arrival time of the tracer front. That is, we first solve the equation

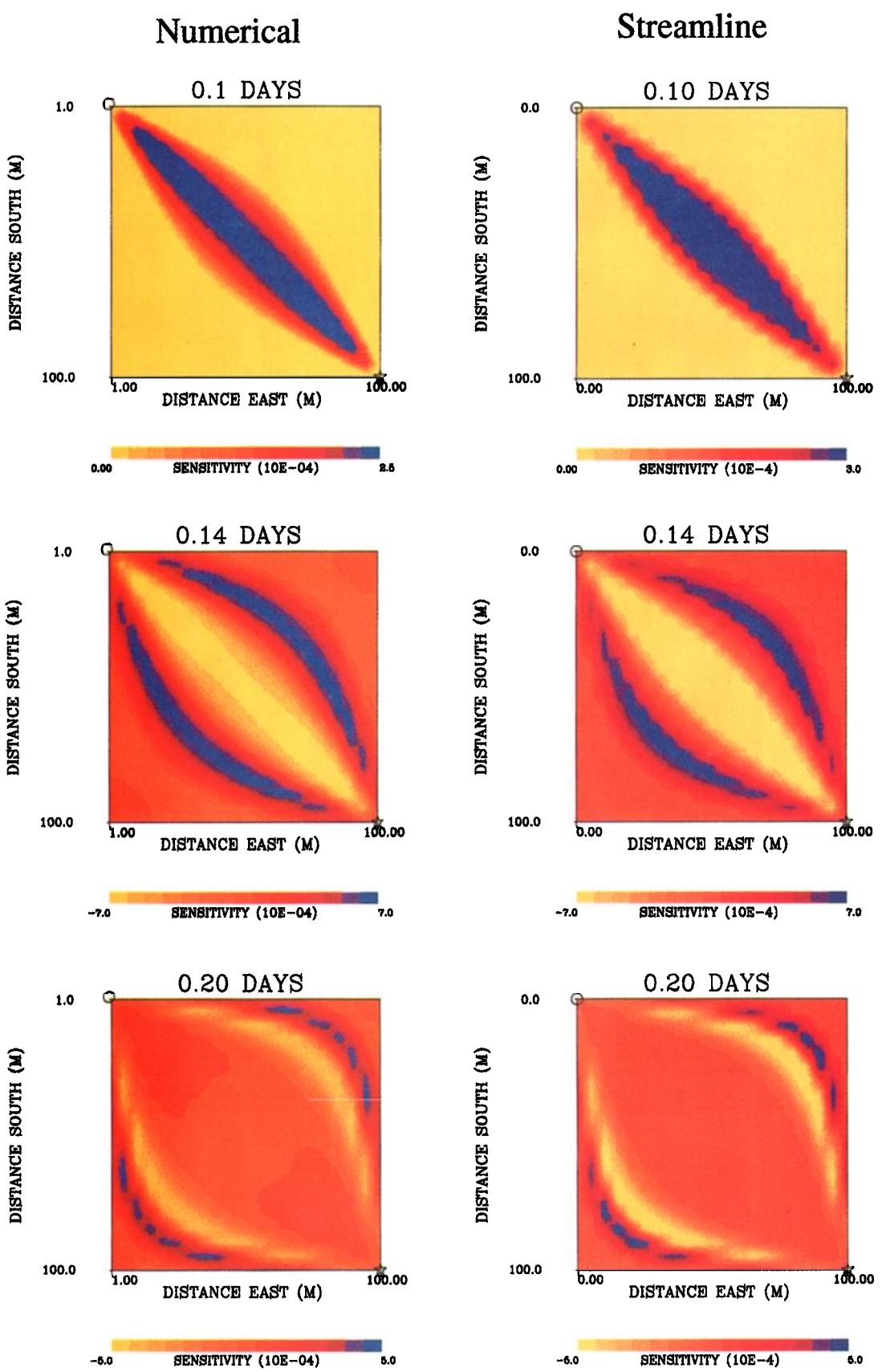

Plate 1. Permeability sensitivities for the three sample points designated in Figure 1. The plate depicts the ratio of perturbation in concentration to the perturbation in permeability. Sensitivities calculated using a numerical perturbation approach (numerical) are compared to those estimated using the asymptotic semi-analytic approach (streamline).

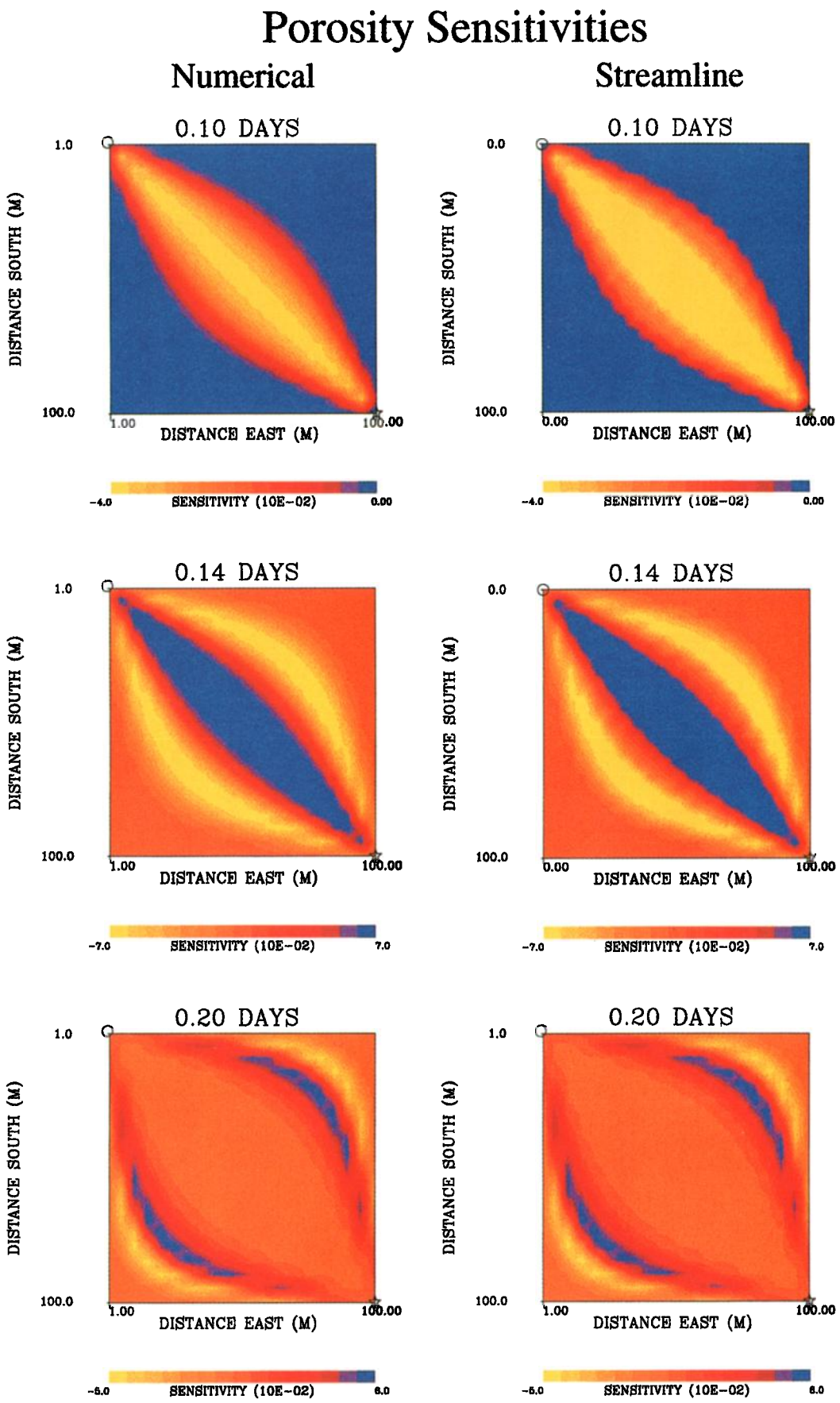

Plate 2. Porosity sensitivities for the three sample points designated in Figure 1.

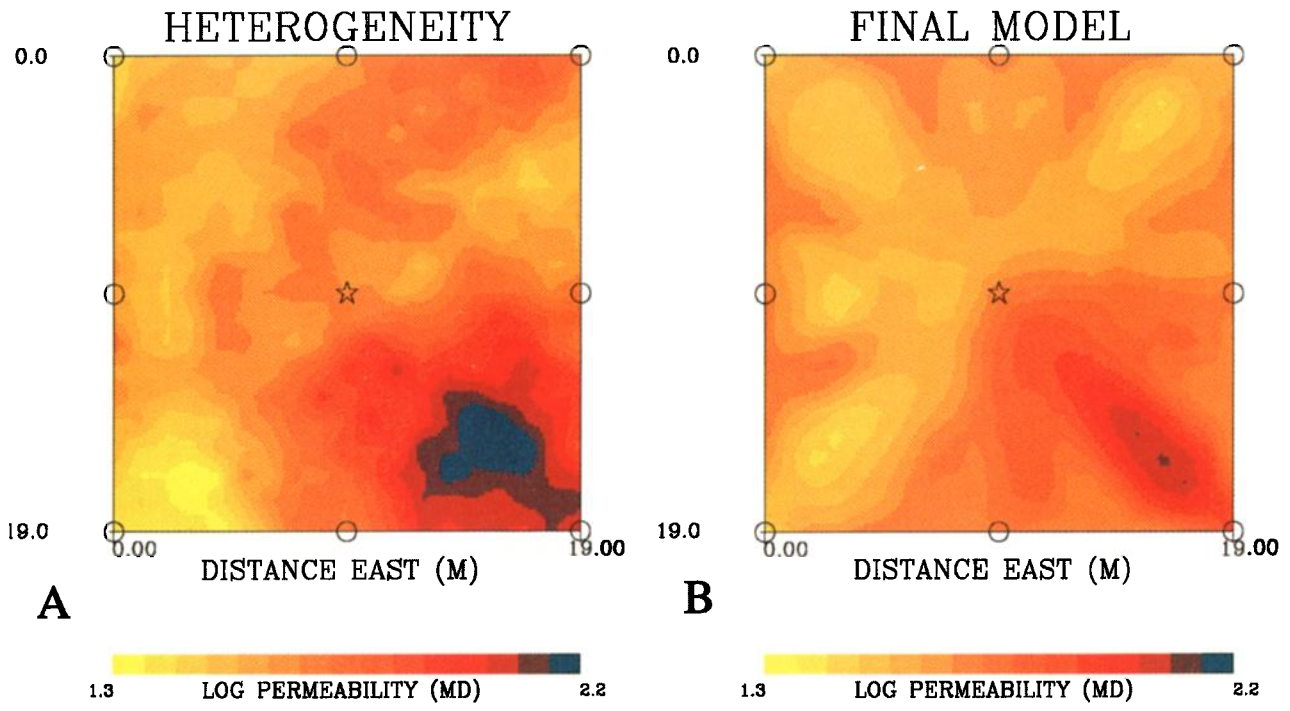

Plate 3. (a) Stochastic realization of spatially correlated random permeability field. The central injection well is indicated by a star, the producing wells are denoted by open circles. The correlation half width was seven grid blocks and the random deviates were drawn from a lognormal distribution. The natural logarithm of the permeabilities are shown. (b) Permeability estimates derived by the iterative inversion algorithm.

$$\delta t_i = \int_{\Sigma_i} \delta s(\mathbf{x})\, dr \tag{26}$$

for an initial distribution of model parameters, using either some measure of "first" arrival time or the arrival time of the maximum peak as the basic datum. This is also a nonlinear inverse problem, solved by iterative linearization, but in our applications the arrival time problem seemed to be much less sensitive to the starting model and less likely to be trapped in a local minimum. The arrival time inversion "lines up" the tracer concentration curves, providing an initial permeability, porosity, and pressure gradient model. Using these starting values we could then fit the concentration data quite well. The initial inversion step is to find permeability, porosity, and pressure gradient distributions to match the travel time residuals

$$\delta \mathbf{t} = \mathbf{S}\delta\mathbf{p} \tag{27}$$

where $\delta\mathbf{t}$ are the travel time residuals, $\mathbf{S}$ is the matrix whose entries are the sensitivity coefficients, and $\delta\mathbf{p}$ are the model parameters, the porosity, permeability, and pressure gradient magnitude deviations in each grid block. The sensitivity coefficients for a particular grid block are simply the integration of the partial derivatives in equation (21) over the streamline segments intersecting that grid block. As in many other inverse problems [*Tarantola*, 1987; *Parker*, 1994] the system of equations (27) is underdetermined, and no unique solution exists. Numerically, this means that estimates of the model parameters will be unstable: Small perturbations of the data will produce large changes in model parameter estimates. This instability may be overcome by imposing additional constraints on the set of possible solutions. The constraints are often in the form of regularization or penalty terms [*Parker*, 1994; *Vasco et al.*, 1997a]. For example, in grid blocks which do not influence the data significantly we may wish to bias the permeability and porosity to the background values of the initial model which we denote by $\mathbf{p}^0$. This may be done by minimizing the quantity $|\mathbf{p} - \mathbf{p}^0|^2$ in addition to satisfying (27). Other considerations are possible, for example we may feel that the structure should be smoothly varying laterally if that is compatible with the observations. Thus we might minimize some measure of spatial difference between adjacent grid blocks [*Tarantola*, 1987; *Parker*, 1994].

The two-step approach (travel time–concentration history) was used to match the tracer concentration histories. The record of mean squared tracer misfit as a function of iteration is shown in Figure 2. The initial fits to the tracer data, based upon a uniform layer are shown in Figure 3a. The initial calculated breakthroughs contain large offsets from the synthetic tracer curves. The initial 11 iterations entailed matching the arrival times and the subsequent iterations involve matching the concentration histories themselves. The single greatest reduction in misfit occurs in matching the arrival times. The subsequent steps, matching concentration history, reduce the misfit to a very small value. The resulting matches, shown in Figure 3b, are quite good, with no indication of matching secondary peaks. The resulting permeability estimates (Plate 3b) share many gross features with the permeability distribution used to generate the synthetic data (Plate 3a). In particular, the high-permeability zone in the southeast is recovered as is the low-permeability feature extending from the southwest to the northeast. The arrival time fitting step proved critical to recovering the large-scale variations in permeability

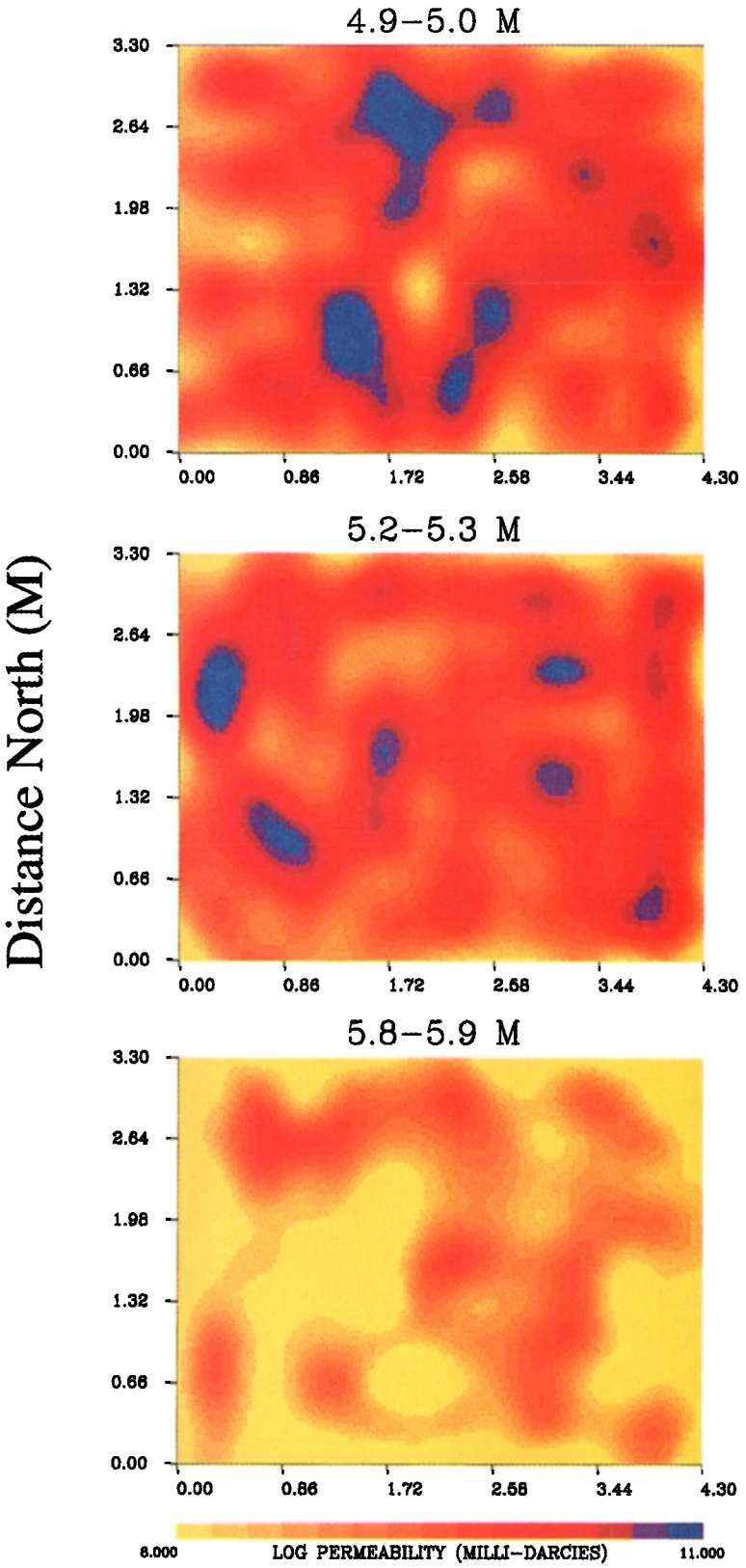

Plate 4. Permeability variations for three depth ranges in the test cell at Hill AFB. The natural logarithm of the permeabilities are shown.

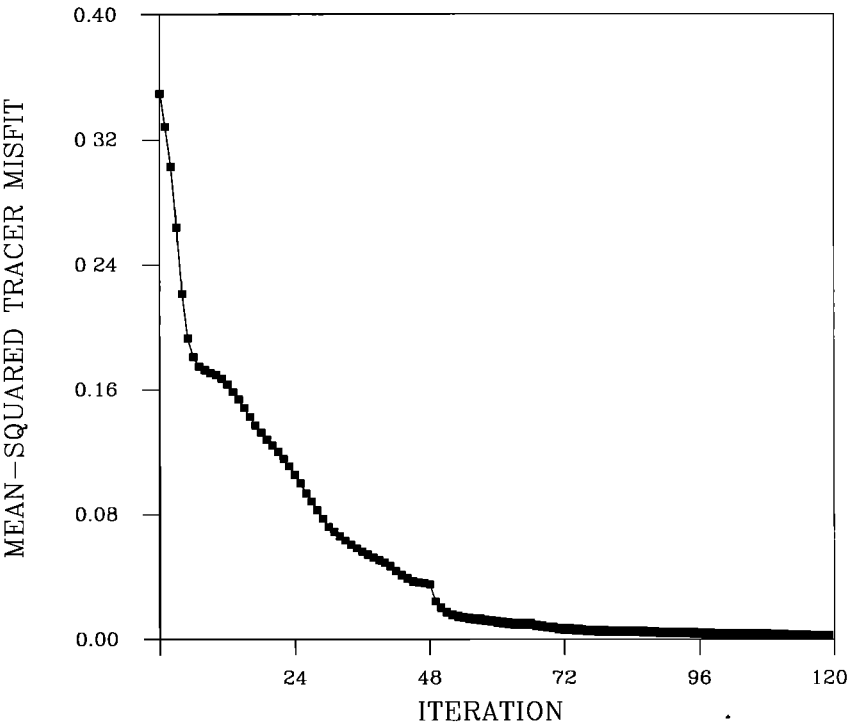

Figure 2. The mean-squared misfit to the tracer data as a function of the number of linearized iterations. The first 11 points correspond to matching the travel times, while subsequent points correspond to matching the tracer concentration histories.

between the boreholes. We should note that the tracer inversion can only recover the gross variation of permeability between the wells. The distribution in Plate 3b is a smeared version of the true permeability structure. The primary reason for the smearing is that the sensitivities, as shown in Plate 1, are themselves elongated between well pairs, producing extensive lateral averaging. Owing to the well configuration, it is not possible to recover the fine details of the permeability variation. We should note that with more extensive data sets, for example, multiple experiments in which the flow structures are transverse, it is possible to recover smaller-scale variations. This points to the importance of solution assessment, determination of the resolution and uncertainty associated with model parameter estimates [*Vasco et al.*, 1997a]. Owing to space limitations, we do not have time to address this important topic.

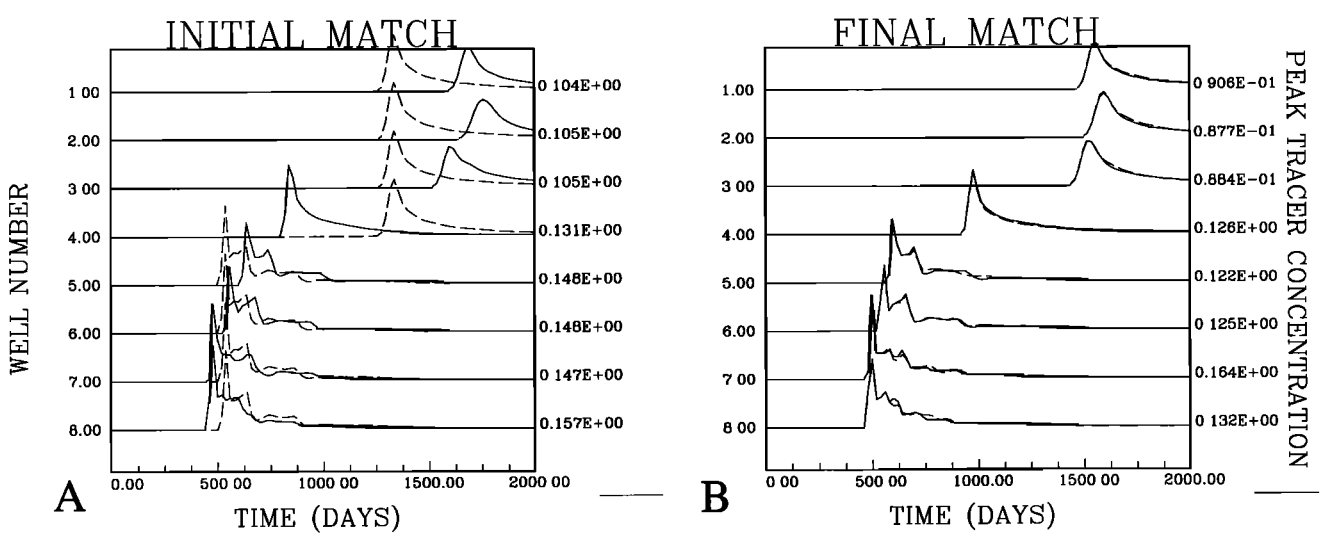

Figure 3. (a) Tracer concentration histories for the eight producing wells of the nine spot (solid lines). Also shown are predicted concentration histories based upon a uniform permeability distribution of 5 mdarcies (dashed lines). (b) Synthetic tracer concentrations, as in Figure 3a (solid lines), and tracer concentrations predicted by the solution of the inverse problem (dashed lines).

4. Application: The Hill Air Force Base Experiment

Non–aqueous phase liquid (NAPL) contamination of groundwater is a widespread and difficult problem. Because NAPLs may remain for extended periods of time and slowly dissolve into infiltrating rainwater, they present a significant threat to water quality. Quantifying the amount and the spatial distribution of NAPL trapped in porous media at hazardous waste sites is of great importance in determining its environmental impact and in selecting appropriate remediation strategies. Recently the use of partitioning interwell tracer tests (PITT) has shown great promise in this regard [*Pope et al.*, 1994; *Jin et al.*, 1995]. The approach involves injection of a suite of conservative and reactive, or "partitioning," tracers into wells located at the waste site. The tracer response is monitored at extraction wells. During the transport, the partitioning tracers are retarded by interaction with the NAPL present while the conservative tracers are not delayed. The conservative tracer response can be used to estimate subsurface property variations such as porosity and permeability distribution. The "chromatographic separation" between the conservative and partitioning tracers can be utilized to estimate subsurface distribution of NAPL [*Pope et al.*, 1994; *James et al.*, 1997].

Recently, several innovative cosolvent flushing and partitioning tracer experiments have been carried out at the Hill AFB, Utah [*Annable et al.*, 1994; *Rao et al.*, 1997]. The goal is to develop minimally invasive techniques for detecting and removing NAPL contaminants. In this section we shall examine a nonpartitioning tracer experiment using a conservative tracer (Bromide) to characterize the distribution of permeability and porosity in the subsurface prior to the partitioning tracer and cosolvent-flushing experiments. We shall use the asymptotic sensitivity estimates as a basis for an inversion of the Bromide tracer data.

4.1. Site Description and Experimental Design

The tests at Hill AFB are, in part, the response to a number of contaminated sites on the base itself. The operable unit 1 contains two chemical disposal pits, which contain predominantly aviation fuels and chlorinated solvents used during the 1940s and 1950s. Also, a nearby former fire training area may contribute unextinguished fuels and combustion byproducts to the groundwater in the test area. The aquifer consists of sands, gravels (with some large cobbles), and clays with a mean permeability of 20 darcies. The base of the aquifer is defined by an impermeable clay layer. The NAPL, which is lighter than water, is in the form of a plume covering several acres (1 acre equals 0.405 ha, or 4047 m^2) [*Annable et al.*, 1994].

An isolation test cell was installed for the purpose of evaluating the use of cosolvents as a remediation tool. The cell, consisting of a sealable sheet pile barrier system, measures 3.5 by 4.3 m and extends to a depth of 9.1 m below the ground surface, some 3 m below the confining unit of the aquifer. Four injection wells were installed at one end of the cell and three extraction wells emplaced at the opposite edge. In between, 12 multilevel samplers were installed to monitor the tracer/contaminant changes within the cell (Figure 4). The samplers formed a roughly uniform grid with vertical positions between 4.6 and 6.1 m below the ground, at a spacing of 0.4 m. Following the installation of the samplers, the water table was raised to 4.5 m.

The details of the tracer tests are given by *Annable et al.*

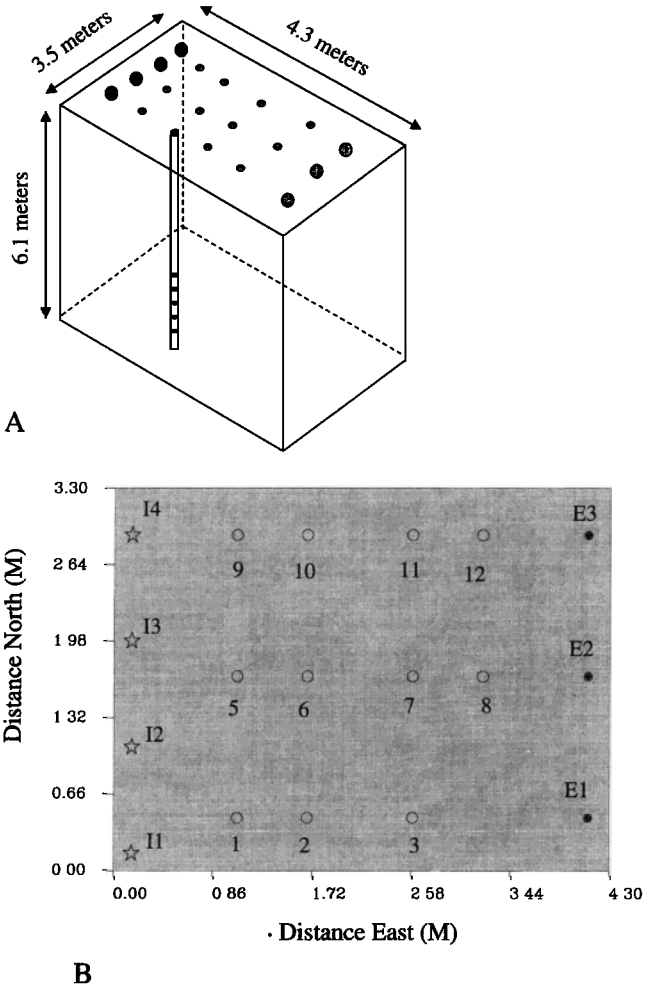

Figure 4. (a) Schematic diagram of the Hill AFB test cell (not to scale). (b) Location map indicating the positions of the four injection wells (I1, I2, I3, and I4), the wells containing multilevel samplers, and the three extraction wells (E1, E2, and E3) in the Hill AFB test cell. The shaded rectangle outlines the test cell itself.

[1994] and *Rao et al.* [1997]. In all, five tracers (bromide, ethanol, n-pentanol, n-hexanol, and 2,2-dimethyl-3-pentanol) were released in the experiment. The nonsorbing bromide tracer served to evaluate the hydrodynamic properties of the test cell and to design the partitioning tracer experiments. All tests were conducted over an 8-day period under steady flow conditions. A 0.1 pore volume pulse of a mixture of tracers was introduced over a 3.3-hour period after approximately three pore volumes of continuous flow. The average flow rate of 3.1 L/min produced an average darcy velocity of 0.03 m/h. The bromide concentrations were analyzed at the University of Florida using ion chromatography.

4.2. Inversion of Bromide Tracer Data

In order to obtain a three-dimensional porosity and permeability distribution compatible with the observed bromide concentration histories, we performed an iterative nonlinear inversion. As a first step the test cell was partitioned into a 14 × 11 × 10 grid of nonoverlapping blocks, a total of 1540 volume elements. The spatial dimensions of the cells were 0.30 m laterally, and 0.15 m vertically. The choice of the parameter-

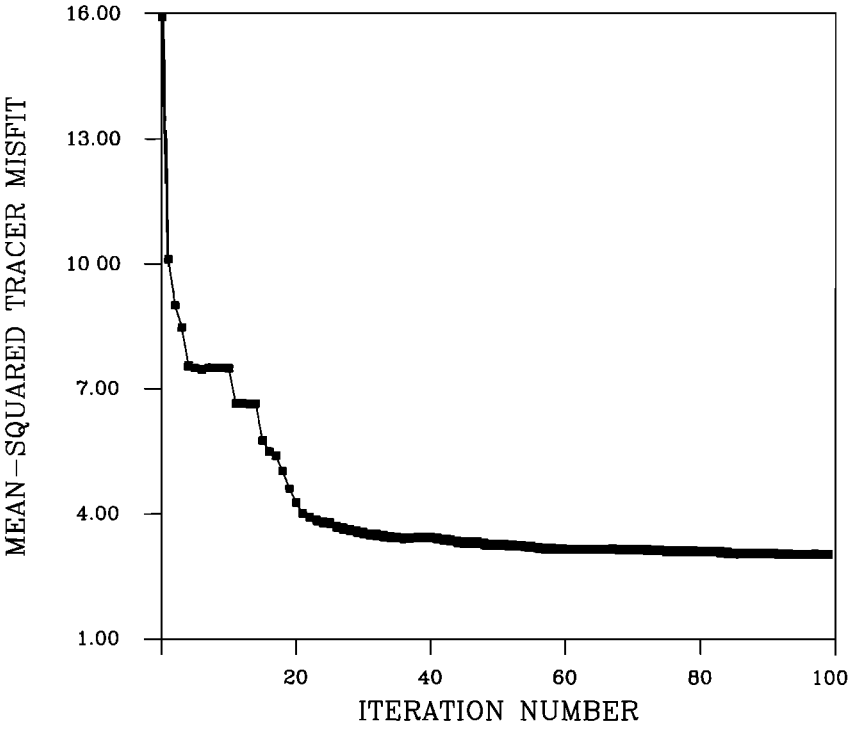

Figure 5. Mean-squared tracer misfit as a function of iteration number. The initial 15 points are associated with a fit to the peak arrival times; the latter points are misfits resulting from a fit to the concentration histories.

ization was dictated by the spacing of multilevel samplers, the observed scale of heterogeneity in the area, and the test cell boundary conditions. In particular, we required enough cells in our model to capture variations between samplers laterally as well as in depth. The external boundary of the model was dictated by the location of the pile barrier system. The initial permeability of each cell was 20 darcies, except for the lowermost layer which was set at 0.001 darcy to reflect the presence of a relatively impermeable clay layer, the lower boundary of the aquifer. The initial porosity was set at 20%, in agreement with core samples from the area. The sheet pile boundaries of the test cell were assumed to prevent flow, providing the boundary conditions for the simulation and inversion.

Given an initial permeability and porosity model and the boundary conditions and flow rates, we calculate the pressure and velocity fields using finite differences and determine some 2000 streamlines through the test cell. With the synthetic case as a guide we first perform an inversion of the first arrival times of the bromide at each sampler and well. Unfortunately, many samplers were not activated in time to record the first appearance of the bromide. Therefore we decided to use the arrival time of the observed maximum of the bromide concentration as the basic datum. Specifically, the difference between the observed and calculated travel times, the travel time residual δt_i in (27), is given by the time associated with the observed maximum minus the time associated with the calculated maximum. We solved the system of equations (27) in a least squares sense [*Parker*, 1994] using the iterative solver LSQR [*Paige and Saunders*, 1982]. In addition to simply finding a model which fit the data we included regularization as discussed in the section describing the synthetic nine-spot inversion. In numerical terms we have to solve an augmented system of equations, where the additional equations are related to the minimization of model deviations from the starting structure $\mathbf{p}^0$. Because the inverse problem is nonlinear, the streamlines depend on the distribution of permeability, porosity, and pressure, and the linearized system of equations must be solved iteratively. At each iteration the streamlines are recalculated and the sensitivity matrix reconstructed and model perturbations relative to the previous permeability and porosity distribution are estimated. The mean-squared error associated with each iteration is shown in Figure 5 for the two-step inversion (travel time, concentration history), the first 15 iterations correspond to the travel time fitting, and subsequent iterations correspond to matching the concentration histories. Ten iterations sufficed to minimize the misfit to the travel time data, and the misfit reduction appears to level off (Figure 5). During the final iterations, in which the concentration histories are matched, gradual misfit reduction takes place (Figure 5). Observed tracer curves for 12 of the multilevel samplers (curves 4–15) and the three extraction wells (curves 1–3) are shown in Figure 6a. Also shown in Figure 6a are the tracer breakthroughs predicted using a uniform permeability of 20 darcies and a porosity of 0.2. There are clear discrepancies between the observed and calculated tracer concentration histories, an indication of the significant lateral and vertical heterogeneity within the test cell. The final matches are shown in Figure 6b for the first 15 of the 44 tracer concentration histories. The fit has improved significantly relative to the initial match (Figure 6a).

Three layers from the permeability distribution derived from the bromide concentration data are shown in Plate 4. There is significant small-scale variability in the estimated permeabilities. Generally, the permeability decreases downward as the lower boundary of the aquifer is approached. There was an attempt to obtain a set of core samples using the cone penetrometer truck for site characterization. However, owing to the presence of large cobbles, this did not prove possible. There-

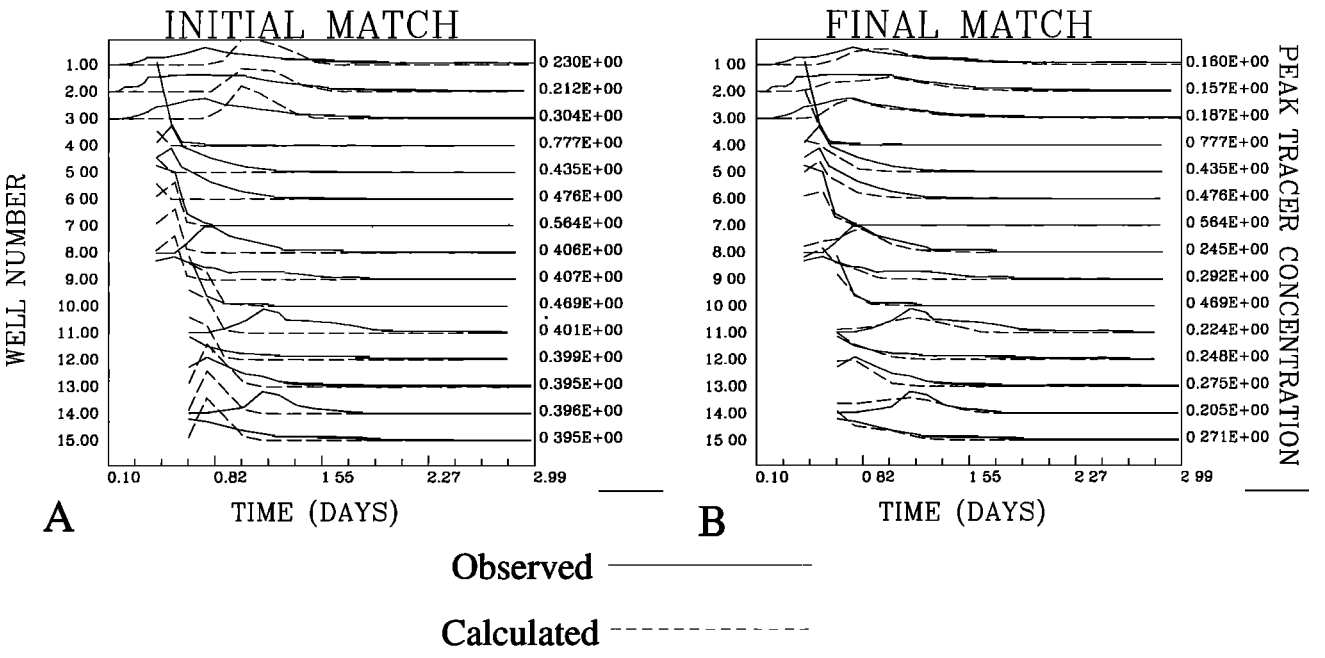

Figure 6. (a) Bromide concentration histories for the first 15 tracer breakthrough curves from the experiment at Hill AFB (solid lines). The dashed lines denote bromide concentrations predicted assuming a uniform permeability distribution of 20 darcies. The well numbers on the left of the panel denote the sampler numbers. The peak observed concentration is indicated to the right of each curve. (b) As in Figure 6a, the first 15 observed (solid line) and calculated (dashed line) bromide concentration histories. The calculated breakthroughs are associated with the final solution of the inversion algorithm.

fore there are no direct measurements of subsurface flow properties. Furthermore, there were no available slug or pump test data to provide an additional check on our permeability estimates. However, the decreasing permeability trend towards the bottom of the test cell is supported by a swept volume calculation for the tracer using moment analysis of the concentration histories [*Harneshaug*, 1997]. An inversion based upon simulated annealing [*Barman et al.*, 1998] produced a model that is qualitatively similar to our results. In particular, the solution contained scattered regions of high permeability, approaching 50 darcies in magnitude. A similar decrease in permeability with depth was also noted.

5. Conclusions

An asymptotic series representation of the concentration history reveals the similarities between the inversion of transport data and tomographic imaging techniques. In particular, the sensitivity coefficients relating perturbations in permeability, porosity, and pressure gradient magnitude to perturbation in concentration are integrals of simple analytic functions over the streamlines. The asymptotic sensitivities match quite closely sensitivities calculated using a perturbation approach.

The computation of the sensitivities relies on a local linearization about an initial permeability and porosity distribution. Each step of the linearized inversion solves for a small perturbation from the previous model. Because our initial model may be quite different from the actual subsurface structure we must procede in an iterative fashion, relinearizing at each step. In practice, we have found an initial arrival time inversion to be critical in the procedure. Matching the concentrations themselves appears to be highly nonlinear and susceptible to local minima. The arrival time matching is much more robust even when the initial model deviates strongly from the final solution. We found this to be true in both the synthetic cases we treated as well as in applying our inversion scheme to field data. In this respect our experience agrees with those involved in the inversion of seismic waveform data [*Zhou et al.*, 1995].

In an actual application the algorithm has performed well, and we deem the two-step linearized inversion a success. The technique proved to be extremely efficient: An inversion for porosity, permeability, and pressure gradient magnitude variations in 1540 grid blocks took less than 1 hour on a standard workstation. In comparison with our previous work on the Hill AFB tracer data, the two-step linearized inversion outperformed a nonlinear conjugate gradient routine [*Vasco et al.*, 1997a], which found a local minimum and matched secondary peaks rather than the actual concentration peaks. Our algorithm also produced a somewhat better match than a simulated annealing algorithm [*Datta-Gupta et al.*, 1995a], which required orders of magnitude more computation (50,000 forward simulation runs). As in any inversion there are issues of resolution and uncertainty associated with our solution [*Vasco et al.*, 1997a]. Owing to space limitations we are not able to treat these topics here. In nonlinear inverse problems there is an additional source of nonuniqueness due to the presence of local minima which we noted above. Assessing solutions to nonlinear inverse problems is an area of active investigation, and we defer to the texts on this topic [*Tarantola*, 1987; *Parker*, 1994].

In our derivation we have neglected dispersion relative to the effect of heterogeneity. However, this is not a fundamental limitation of the method; streamlines and phase fronts exist even in the presence of dispersion, though the front becomes diffuse and it is not possible to define an exact arrival time.

However, it is possible to work with the arrival time of the concentration peak or isoconcentration surfaces and the method may be extended to include longitudinal dispersion along streamlines [*Datta-Gupta and King*, 1995]. For example, any one-dimensional solution of (1) may be used to estimate sensitivities along the streamlines. We have restricted our study to the scalar transport equation, but it is also possible to apply the techniques to systems of partial differential equations, as in electromagnetics [*Kline and Kay*, 1965]. For example, it is possible to consider multiphase flow, such as the propagation of a two-phase front [*Vasco et al.*, 1998]. Such applications are especially appealing for inversion of multiphase production history during petroleum reservoir characterization [*Vasco and Datta-Gupta*, 1997].

Acknowledgments. This work was supported by a Laboratory Directed Research and Development grant from Berkeley Laboratory as well as by funding provided by the Assistant Secretary for Fossil Energy, Office of Oil Gas and Shale Technologies, of the U.S. Department of Energy under contract DE-AC03-76SF00098. Akhil Datta-Gupta would also like to acknowledge financial support from the Office of Environmental Management and the University of Texas at Austin. Computational resources were provided by the Center for Computational Seismology and the National Energy Research Scientific Computing (NERSC) Center of the Berkeley Laboratory. The authors would like to thank Gary Pope at the University of Texas at Austin for many useful discussions and the University of Florida Research group, especially Mike Annable, Wendy Graham, and Suresh Rao, for sharing the Hill tracer test data.

References

Ahlfeld, D. P., J. M. Mulvey, and G. F. Pinder, Designing optimal strategies for contaminated groundwater remediation, *Adv. Water Resour.*, *9*, 77–84, 1986.

Ahlfeld, D. P., J. M. Mulvey, G. F. Pinder, and E. F. Wood, Contaminated groundwater remediation design using simulation, optimization, and sensitivity theory, 1, Model development, *Water Resour. Res.*, *24*, 431–441, 1988.

Aldridge, D. F., Linearization of the eikonal equation, *Geophysics*, *59*, 1631–1632, 1994.

Annable, M. D., P. C. Rao, K. Hatfield, W. D. Graham, and A. L. Wood, Use of partitioning tracers for measuring residual NAPL distribution in a contaminated aquifer: Preliminary results from a field-scale test, paper presented at 2nd Tracer Workshop, I. F. E. Norway, Univ. of Tex., Austin, Nov. 14–15, 1994.

Barman, I., S. Yoon, A. Datta-Gupta, and G. A. Pope, In-situ characterization of residual NAPL distribution by stochastic inverse modeling of partitioning tracer tests, paper presented at *SPE/EPA Explor. and Prod. Environ. Conf.*, Feb. 28 through March 30, Austin, Tex., 1998.

Bear, J., *Dynamics of Fluids in Porous Media*, Dover, Mineola, N. Y., 1972.

Carter, R. D., L. F. Kemp Jr., and A. C. Pearce, Discussion of comparison of sensitivity coefficient calculation methods in automatic history matching, *Soc. Petrol. Eng. J.*, *22*, 205–208, 1982.

Cerveny, V., I. A. Molotkov, and I. Psencik, *The Ray Method in Seismology*, Charles Univ. Press, Prague, 1978.

Chang, L.-C., C. A. Shoemaker, and P. L.-F. Liu, Optimal time-varying pumping rates for groundwater remediation: Application of a constrained optimal control algorithm, *Water Resour. Res.*, *28*, 3157–3173, 1992.

Datta-Gupta, A., and M. J. King, A semianalytic approach to tracer flow modeling in heterogeneous permeable media, *Adv. Water Resour.*, *18*, 9–24, 1995.

Datta-Gupta, A., L. W. Lake, and G. A. Pope, Characterizing heterogeneous permeable media with spatial statistics and tracer data using sequential simulated annealing, *Math. Geol.*, *27*, 763–787, 1995a.

Datta-Gupta, A., D. W. Vasco, and J. C. S. Long, Sensitivity and spatial resolution of transient pressure and tracer data for heterogeneity characterization, *SPE Form. Eval.*, *12*(2), 625–637, 1995b.

Fatemi, E., B. Engquist, and S. Osher, Numerical solution of the high frequency asymptotic expansion for the scalar wave equation, *J. Comp. Phys.*, *120*, 145–155, 1995.

Gelhar, L. W., and C. L. Axness, Three-dimensional stochastic analysis of macrodispersion in aquifers, *Water Resour. Res.*, *19*, 161–180, 1983.

Gelhar, L. W., and M. A. Collins, General analysis of longitudinal dispersion in nonuniform flow, *Water Resour. Res.*, *7*, 1511–1521, 1971.

Golub, G. H., and C. F. Van Loan, *Matrix Computations*, John Hopkins Univ. Press, Baltimore, Md., 1989.

Gorelick, S. M., C. I. Voss, P. E. Gill, W. Murry, M. A. Saunders, and M. H. Wright, Aquifer reclamation design: The use of contaminant transport simulation combined with nonlinear programming, *Water Resour. Res.*, *20*, 415–427, 1984.

Graham, W. D., and D. Mclaughtlin, Stochastic analysis of nonstationary subsurface solute transport, 1, Unconditional moments, *Water Resour. Res.*, *25*, 215–232, 1989a.

Graham, W. D., and D. Mclaughlin, Stochastic analysis of nonstationary subsurface solute transport, 2, Conditional moments, *Water Resour. Res.*, *25*, 2331–2355, 1989b.

Grundy, R. E., C. J. van Duijn, and C. N. Dawson, Asymptotic profiles with finite mass in one-dimensional contaminant transport through porous media: The fast reaction case, *Q. J. Mech. Appl. Math.*, *47*, 69–106, 1994.

Harneshaug, T., Permeability and saturation distributions from tracer data, M.S. thesis, Univ. of Tex., Austin, 1997.

Hyndman, D. W., J. M. Harris, and S. M. Gorelick, Coupled seismic and tracer test inversion for aquifer property characterization, *Water Resour. Res.*, *30*, 1965–1977, 1994.

Jacquard, P., and C. Jain, Permeability distribution from field pressure data, *Soc. Pet. Eng. J.*, *5*, 281–294, 1965.

Jaekel, U., A. Georgescu, and H. Vereecken, Asymptotic analysis of nonlinear equilibrium solute transport in porous media, *Water Resour. Res.*, *32*, 3093–3098, 1996.

James, A. I., W. D. Graham, K. Hatfield, P. S. C. Rao, and M. D. Annable, Optimal estimation of residual non-aqueous phase liquid saturations using partioning tracer concentration data, *Water Resour. Res.*, *33*, 2621–2636, 1997.

Jin, M., M. Delshad, V. Dwarakanath, D. C. McKinney, G. A. Pope, K. Sepehrnoori, and C. E. Tilburg, Partitioning tracer test for detection, estimation, and remediation performance assessment of subsurface nonaqueous phase liquids, *Water Resour. Res.*, *31*, 1201–1211, 1995.

Kabala, Z. J., and P. C. D. Milly, Sensitivity analysis of flow in unsaturated heterogeneous porous media: Theory, numerical model, and its verification, *Water Resour. Res.*, *26*, 593–610, 1990.

King, M. J., and A. Datta-Gupta, Streamline simulation: A current perspective, *In Situ*, *22*(1), 91–140, 1998.

Kline, M., and I. W. Kay, *Electromagnetic Theory and Geometrical Optics*, John Wiley, New York, 1965.

Knopman, D. S., and C. I. Voss, Behavior of sensitivities in the one-dimensional advection-dispersion equation: Implications for parameter estimation and sampling design, *Water Resour. Res.*, *23*, 253–272, 1987.

Lake, L. W., *Enhanced Oil Recovery*, Prentice-Hall, Englewood Cliffs, N. J., 1989.

Mclaughlin, D. B., and L. R. Townley, A reassessment of the groundwater inverse problem, *Water Resour. Res.*, *32*, 1131–1161, 1996.

Medina, A., and J. Carrera, Coupled estimation of flow and solute transport parameters, *Water Resour. Res.*, *32*, 3063–3076, 1996.

Neele, F., J. C. VanDecar, and R. Snieder, A formalism for including amplitude data in tomographic inversions, *Geophys. J. Int.*, *115*, 482–496, 1993.

Nolet, G., Seismic wave propagation and seismic tomography, in *Seismic Tomography*, edited by G. Nolet, pp. 1–23, D. Reidel, Norwell, Mass., 1987.

Paige, C. C., and M. A. Saunders, LSQR: An algorithm for sparse linear equations and sparse linear systems, *Assoc. Comput. Mach. Trans. Math. Software*, *8*, 195–209, 1982.

Parker, R. L., *Geophysical Inverse Theory*, Princeton Univ. Press, Princeton, N. J., 1994.

Pope, G. A., M. Jin, V. Dwarakanath, B. A. Rouse, and K. Sepehrnoori, Partitioning tracer tests to characterize organic contaminants, paper presented at 2nd Tracer Workshop, I. F. E. Norway, Univ. of Tex., Austin, Nov. 14–15, 1994.

Protter, M. H., and C. B. Morrey, *Modern Mathematical Analysis*, Addison-Wesley, Reading, Mass., 1964.

Rao, P. S. C., M. D. Annable, R. K. Sillan, D. Dai, K. Hatfield, and W. D. Graham, Field-scale evaluation of in situ cosolvent flushing for enhanced aquifer remediation, *Water Resour. Res.*, *33*, 2673–2686, 1997.

Robertson, J. M., *Hydrodynamics: In Theory and Application*, Prentice-Hall, Englewood Cliffs, N. J., 1965.

Rubin, Y., Prediction of tracer plume migration in disordered porous media by the method of conditional probabilities, *Water Resour. Res.*, *27*, 1291–1308, 1991.

Samper, F. J., and S. P. Neuman, Adjoint state equations for advective-dispersive transport, in *Finite Elements in Water Resources: Proceedings of the VI International Conference*, edited by A. Sa da Costa et al., pp. 423–437, Springer-Verlag, New York, 1986.

Sethian, J. A., *Level Set Methods*, Cambridge Univ. Press, New York, 1996.

Skaggs, T. H., and D. A. Barry, Sensitivity methods for time-continuous, spatially discrete groundwater contaminant transport models, *Water Resour. Res.*, *32*, 2409–2420, 1996.

Sun, N.-Z., and W. W.-G. Yeh, Coupled inverse problems in groundwater modeling, 1, Sensitivity analysis and parameter identification, *Water Resour. Res.*, *26*, 2507–2525, 1990.

Tarantola, A., *Inverse Problem Theory: Methods for Data Fitting and Model Parameter Estimation*, Elsevier Sci., New York, 1987.

van der Zee, S. E. A. T. M., Analytical traveling wave solutions for transport with nonlinear and nonequilibrium adsorption, *Water Resour. Res.*, *26*, 2563–2578, 1990.

van Duijn, C. J., and P. Knabner, Traveling waves in the transport of reactive solutes through porous media: Adsorption and binary ion exchange, 1, *Trans. Porous Media*, *8*, 167–194, 1992.

Vasco, D. W., and A. Datta-Gupta, Integrating multiphase production history in stochastic reservoir characterization, *SPE Form. Eval.*, *12*(3), 149–156, 1997.

Vasco, D. W., A. Datta-Gupta, and J. C. S. Long, Resolution and uncertainty in hydrologic characterization, *Water Resour. Res.*, *33*, 379–397, 1997a.

Vasco, D. W., J. E. Peterson, and K. H. Lee, Ground-penetrating radar velocity tomography in heterogeneous and anisotropic media, *Geophysics*, *62*, 1758–1773, 1997b.

Vasco, D. W., S. Yoon, and A. Datta-Gupta, Integrating dynamic data into high-resolution reservoir models using streamline-based analytic sensitivity coefficients, *Proc. of the 1998 Annual Technical Conf. and Exhibit., SPE 49002*, New Orleans, La., 1998.

Vemuri, V., and W. J. Karplus, Identification of nonlinear parameters of groundwater basins by hybrid computation, *Water Resour. Res.*, *5*, 172–185, 1969.

Yeh, W. W.-G., Review of parameter identification procedures in groundwater hydrology: The inverse problem, *Water Resour. Res.*, *22*, 95–108, 1986.

Zhou, C., W. Cai, Y. Luo, G. T. Schuster, and S. Hassanzadeh, Acoustic wave-equation traveltime and waveform inversion of crosshole seismic data, *Geophysics*, *60*, 765–773, 1995.

A. Datta-Gupta, Department of Petroleum Engineering, Texas A&M University, College Station, TX 77843. (e-mail: datta-gupta@spindletop.tamu.edu)

D. W. Vasco, Earth Sciences Division/Building 90, Berkeley Laboratory, 1 Cyclotron Road, Berkeley, CA 94720. (e-mail: dwvasco@lbl.gov)

(Received December 30, 1997; revised August 20, 1998;
accepted August 21, 1998.)